sustainability

MDPI

Article

Combined Effects of the Surface Urban Heat Island with Landscape Composition and Configuration Based on Remote Sensing: A Case Study of Shanghai, China

Hongyu Du [1,*], Jinquan Ai [2], Yongli Cai [3,4,*], Hong Jiang [5] and Pudong Liu [6,7]

1 Institute of Ecology and Sustainable Development, Shanghai Academy of Social Sciences, N0. 622, Middle Huaihai Road, Huangpu District, Shanghai 200020, China
2 Faculty of Geomatics, East China University of Technology, Nanchang 330013, China; jinquan@ecit.cn
3 Shanghai Key Laboratory for Urban Ecological Processes and Eco-Restoration, East China Normal University, Shanghai 200241, China
4 Department of Environmental Science, East China Normal University, No. 500, Dongchuan Road, Minhang District, Shanghai 200241, China
5 Institute of Ecology Engineering, Guizhou University of Engineering Science, Bijie 51700, China; hongjll@126.com
6 School of Surveying and Geoinformatics, Shandong Jianzhu University, Jinan 250101, China; liupudong@yeah.net
7 The Department of Automation, Qingdao University, Qingdao 266071, China
* Correspondence: duhongyu@sass.org.cn (H.D.); ylcai@geo.ecnu.edu.cn (Y.C.)

Received: 21 March 2019; Accepted: 17 May 2019; Published: 21 May 2019

check for updates

Abstract: Rapid urbanization leads to changes in surface coverage and landscape patterns. This results in urban heat island (UHI) effects and a series of negative ecological consequences. Considering this concern and taking Shanghai as an example, this paper concentrates on the effects of surface coverage and landscape patterns on urban land surface temperature (LST). The research is based on quantitative retrieval of remote sensing data with consideration of methods in multiple disciplines, including landscape ecology, geographic information systems, and statistical analysis. It concludes that, over time, the thermal environment of Shanghai is becoming critical. The average LST ranking of different surface coverage is as follows: Construction land (CL) > bare land (BL) > green land (GL) > agricultural land (AL) > water body (WB). LST varies significantly with the type of surface coverage. CL contributes the most to the UHI, while WB and GL have obvious mitigation effects on the UHI. The large area, low degree of landscape fragmentation, and complex outlines lead to low LST rankings for GL, WB, and AL and a high LST ranking for CL. The conclusions indicate that CL should be broken down by GL and WB into discrete pieces to effectively mitigate UHI effects. The research reveals UHI features and changes in Shanghai over the years and provides practical advice that can be used by urban planning authorities to mitigate UHI.

Keywords: land surface temperature; land cover types; landscape pattern; urban heat island; remote sensing; Shanghai

1. Introduction

During the process of urbanization, the natural land cover changes to artificial surfaces on a large scale. The increased artificial surfaces have different thermal capacities, reflection rates, aerodynamics, and levels of evaporation [1,2]. This leads to urban heat island (UHI) effects, which cause a series of ecological consequences, such as the formation of hazy weather, the deterioration of air quality, and extra urban energy consumption [3,4]. Therefore, mitigating UHI has become one of the most important topics in the fields of urban ecology, urban landscaping, urban geography, and urban meteorology.

Changes to the underlying surface are the main cause of UHI effects. Therefore, it is significant to explore the relationship between the underlying surface and the urban thermal environment. At present, there is a lot of research focusing on this field [5–7]. The research of [8] shows that land surface temperature (LST) is significantly positively correlated with the normalized difference buildup index (NDBI) and negatively correlated with the normalized difference vegetation index (NDVI). Previous studies also showed that underlying landscape patterns have an important influence on LST [9,10]. The authors of [11] took the Aksu oasis in northwest China as an example to study the influence of green space on surface temperature. The research results show that the area ratio of green space patches in the landscape is the most important factor. Asgarian showed that increasing the connectivity and complexity of urban landscapes can increase LST, which is caused by the high energy exchange between different landscape units [12]. The conclusion of [13] shows that the loss of green space leads to a major LST increase, while green space expansion generates an LST decrease. However, most research in this field concentrates on the relationship between LST and land cover types or area. In-depth research of the relationship between LST and the landscape patterns of land coverage types still needs to be improved.

At present, the research methods of UHI effects include traditional ground observations [14], numerical simulations [15,16], and remote sensing [17]. Traditional ground observations involve the collection of data from meteorological observation stations or artificial ground observation points. Then, UHI effects are explored by climatology and statistics. This method has the advantage of continuity and controllability, but only rough spatial distribution of UHI can be obtained due to the limited number of observation points [18]. Numerical simulation can be used to simulate the urban thermal environment. This method has the advantage of continuity, and the mechanism of thermal environmental change can be quantitatively analyzed. However, the disadvantage is uncertainty of model parameters [19]. Remote sensing (RS) monitoring obtains surface temperatures through remote sensors on satellites. This method has continuity, integrity, and real-time data acquisition, overcoming the disadvantages of traditional ground observation and providing more scientific data support for study [20]. At present, common RS image data sources include NOAA/AVHRR, Terra and Aqua/MODIS, Terra and Aqua/ASTER, Landsat/TM and ETM+ and OLI/TIRS. The thermal infrared band of Landsat TM/TM+/OLI/TIRS data has high spatial resolution and geometric accuracy, so it is widely applied in urban thermal environment analysis and served as a database for this research. UHI research based on RS images and LST retrieval uses surface UHI, which is different from air UHI. Unless otherwise mentioned, the UHI in this research indicates only surface UHI.

Shanghai is one of the most urbanized and developed cities in China. In recent years, along with fast urbanization, the thermal environment problem has become serious. The average temperature in summer rises continuously [21–23]. The research of [24] shows that, since the 1980s, the UHI area has increased by more than 700 square kilometers, and the average temperature has increased by 0.9 °C. The research of [25] shows that the average maximum temperature in the Shanghai area fluctuates steadily in summer, but the UHI strength shows a rising trend. Combined with hazy, high-temperature weather, UHI threatens residential life. The study of [26] indicates that UHI enhances the negative impact of a high-temperature climate on residential health and is one of the key factors of the death rate in Shanghai in summer. Improving the urban thermal environment is a common topic of concern for the government and citizens. It is important to accomplish this by optimizing urban planning according to the relationship between LST and underlying coverage.

Taking Shanghai as an example, this study first explores the patterns of spatial and temporal changes in LST rankings in the past 15 years. Then, a model of the areas and patterns of different land cover types and corresponding LST rankings is built. This study can provide a reference for Shanghai and other megacities to improve the living environment, mitigate the UHI effect, and optimize landscape planning.

2. Data and Methods

2.1. Study Area

Shanghai is located in the Yangtze River Delta. It sits on the south edge of the Yangtze River estuary and in the middle portion of the east coast of China (Figure 1). It has 16 districts, with a total area of 6340.5 km^2, a length of 120 km from north to south, and a width of 100 km from east to west.

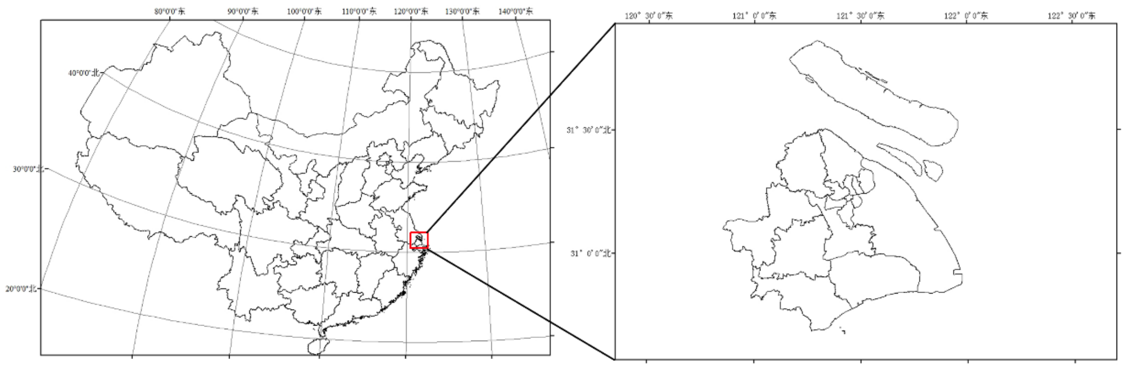

Figure 1. Location map of Shanghai, China.

The population expands continuously. By the end of 2015, the permanent resident population was 24.152 million, including a census-registered population of 14.4297 million.

2.2. Data

In this study, two major datasets were applied: LST and land cover type (LCT).

The LST data, at thermal infrared spatial resolutions of 100 m and 120 m, were obtained from Landsat-8 TIRS and TM/ETM+. In order to unify spatial resolution, the 120 m resolution was resampled to 100 m. Retrieval of LST was based on the atmospheric radiation transfer equation [27]. Initially, a four-year interval between 2000 to 2016 was selected. However, in order to unify the weather background to study UHI, the RS image for each year was sampled in July and August, when Shanghai is the hottest, with sunny weather and no clouds or wind. Finally, RS images from 2000, 2004, 2007, and 2015 were selected. Information on the selected images and the average temperature in July and August of each year from the meteorological station are listed in Table 1.

Table 1. Data source information on remote sensing images.

Satellite Sensor	Orbiter	Date	Quality	Av. Temp. July	Av. Temp. August
Landsat-7 ETM+	118/38, 118/39	2000.08.01	No cloud	29.5 °C	28.6 °C
Landsat-5 TM	118/38, 118/39	2004.07.19	No cloud	30.2 °C	29.4 °C
Landsat-5 TM	118/38, 118/39	2007.07.28	No cloud	30.4 °C	29.7 °C
Landsat-8 OLI/TIRS	118/38, 118/39	2015.08.03	No cloud	30.5 °C	31.2 °C

Source: http://glovis.usgs.gov/.

After retrieval, the LST was classified into seven types by standard deviation classification according to Equation (1), where D is the boundary of each type, a is an integer from one to three, X is the average LST of the image, and S is the standard deviation:

$$D = X \pm aS \tag{1}$$

The LCT data, with a spatial resolution of 30 m, were obtained from remote sensing images by supervised classification [28]. In order to improve the accuracy of the classification results, the LCT data of Shanghai (Figure 2) from 2000, 2004, 2007, and 2015 were obtained through manual visual interpretation and corrected based on high-resolution Google Earth images. Field trips were also conducted when images could not clearly indicate land cover. LCT was classified into five types: Construction land (CL), green land (GL), wetland (WL), agricultural land (AL), and bare land (BL) (see Table 2).

Table 2. Classification of urban land use types.

Abbreviation	Land Cover Type	Description
CL	Construction land	Urban built-up areas, including residential land, commercial land, road land, storage land, industrial land, and public service land
GL	Green land	Any type of vegetation that provides shade, including all trees and shrubs
WL	Wetland	All water body types, including lakes, rivers, wetlands, ponds, etc.
AL	Agricultural land	All agricultural land
BL	Bare land	Unused land, including sand and bare land

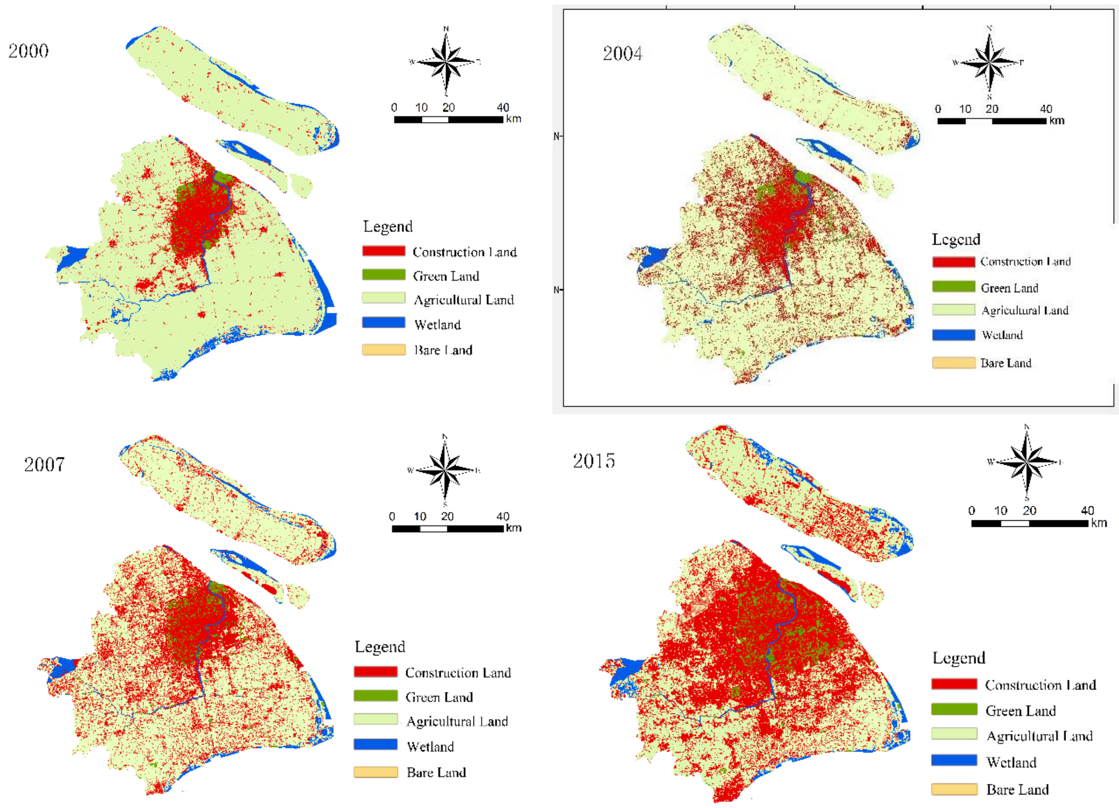

Figure 2. Map of land use in different years.

2.3. Landscape Pattern Index

Indices were selected from patch type and landscape level to quantitatively describe the landscape pattern characteristics of LCT. Landscape level indices are used to describe the overall characteristics of LCT status, while patch type indices focus on the number, morphology, and structure of LCT types. The selected landscape indices include percent landscape (PL), landscape shape index (LSI), number of patches (NP), largest patch index (LPI), and mean Euclidean nearest-neighbor distance (ENN_MN) (Table 3). These are common and frequently used indices in landscape research.

Table 3. Landscape pattern indices used in this study.

Landscape Pattern	Metric (Abbreviation)	Description
Composition	Percent landscape (PLAND)	Proportion of landscape type to total landscape (%)
Configuration	Landscape shape index (LSI)	Perimeter of patch divided by perimeter of circle with the same area as the patch
	Number of patches (NP)	Count of total number of patches
	Largest patch index (LPI)	Area ratio of largest patch in landscape to study area (%)
	Mean Euclidean nearest-neighbor distance (ENN_MN)	Mean distance to nearest neighboring patch of landscape type based on edge-to-edge distance (m)

2.4. Statistical Analysis

In order to study the quantitative relationship between the underlying surface coverage area, landscape pattern index, and LST, the fishing net function of ArcGIS was utilized to extract 6×20 samples in the north–south direction and 5×20 samples in the east–west direction of the study area with a grid unit of 3000 m × 3000 m. Excluding the crossing points, 190 grid samples of 3000 m × 3000 m were obtained. Then, the sampled fields were superimposed with the LST and LCT vector map, respectively, and converted into a grid file (Figure 3). The grid data were input into Fragstats 4.2 to calculate the landscape pattern indices. Finally, the relationship between the average temperature in 190 grids and the landscape pattern indices was calculated in SPSS 19.0.

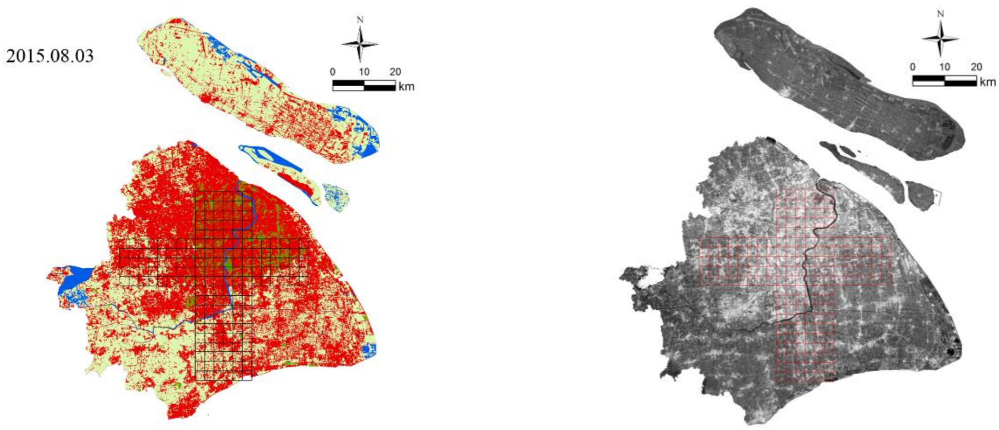

(**a**) (**b**)

Figure 3. Diagram of sample grid in the study area. (**a**) Slice of LCT figure (**b**) Slice of LST greyscale figure.

3. Results

3.1. Characteristics of LST

Based on the method in Section 2.2, the LSTs and temperature classifications of Shanghai in 2000, 2004, 2007, and 2015 were obtained (Figure 4). The LSTs of different LCTs were also calculated, as shown in Table 4.

According to Table 1, the average temperature of Shanghai in July and August increased significantly, from 29.5 °C and 28.6 °C in 2000 to 30.5 °C and 31.0 °C in 2015, respectively.

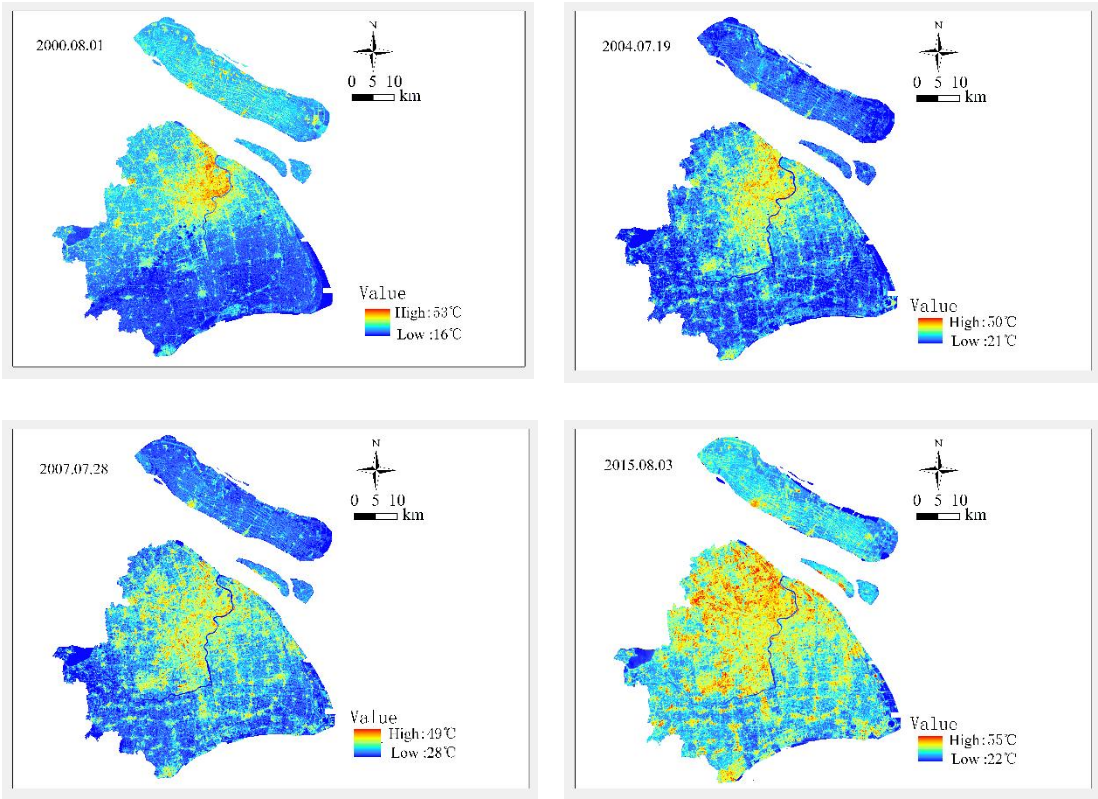

Figure 4. Results of land surface temperature measurement in Shanghai, 2007 and 2015.

The LSTs of different LCTs are quite different. The average LST ranking of all LCTs for all years is: CL > BL > GL > AL > WB. CL has the highest LST, while WB has the lowest. GL, AL, and WB are significantly lower, and CL and BL are significantly higher than the average LST of Shanghai.

Table 4. Land surface temperature (LST) of different land use types through the years (°C).

Year (LST °C)		AL	GL	CL	BL	WL
2000 (31.71)	Minimum	20.67	20.17	22.35	26.41	11.78
	Maximum	36.39	39.26	53.93	50.35	33.69
	Average	30.06	30.14	35.43	33.99	28.93
2004 (34.05)	Minimum	22.42	24.62	25.52	27.61	20.14
	Maximum	38.23	36.76	51.37	43.94	39.48
	Average	32.87	33.18	36.54	35.63	32.03
2007 (35.34)	Minimum	28.58	28.75	27.41	31.03	26.78
	Maximum	48.6	47.12	51.73	48.75	46.23
	Average	34.19	34.38	37.69	36.89	33.55
2015 (35.98)	Minimum	18.05	31.79	29.97	32.02	22.52
	Maximum	51.59	43.68	54.22	43.68	42.02
	Average	35.16	35.21	39.05	37.19	33.29

3.2. Characteristics of LCT

Table 5 shows the area proportions of different LCTs. It indicates that percent of agricultural land (PerAL), percent of wetland (PerWL), and percent of bare land (PerBL) decreased over the years from 37.95%, 25.19%, and 3.74% in 2000 to 21.71%, 12.36%, and 0.36% in 2015, respectively. Percent of green land (PerGL) and percent of construction land (PerCL) increased from 7.81% and 25.31% in 2000 to 24.87% and 40.70% in 2015, respectively.

Table 5. Percentage of land use over the years. PerAL, percent of agricultural land; PerGL, percent of green land; PerCL, percent of construction land; PerBL, percent of bare land; PerWL, percent of wetland.

Year	PerAL	PerGL	PerCL	PerBL	PerWL
2000	37.95	7.81	25.31	3.74	25.19
2004	35.15	12.00	29.14	1.68	24.03
2007	32.97	14.11	36.81	1.27	14.84
2015	21.71	24.87	40.70	0.36	12.36

3.3. Quantitative Relationship Between LST and LCT

The quantitative relationship between LST and LCT was studied based on data of 3 August 2015.

According to Figure 5, there is a good linear relationship between LST and the area ratios of CL, GL, AL, and WB. The fitting equation passes the significance test of 0.05, which indicates that these four LCTs can well explain the change of average LST.

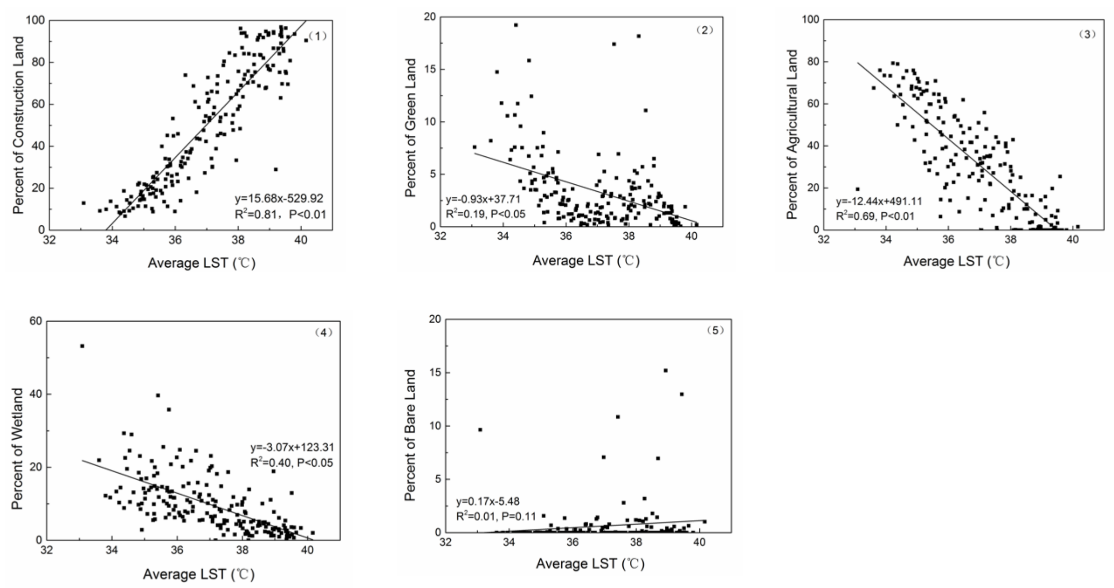

Figure 5. Fitting for land surface temperature and land use type area ratio.

The linear fitting equation of average LST and PerCL is the best (y = 15.68x − 529.92, R^2 = 0.81), indicating a significant positive correlation between them. CL has the greatest influence on LST. A large PerCL leads to high LST. Mean LST is significantly negatively correlated with PerAL (y = −12.44x + 491.11), PerBL (y = −0.93x + 37.71), and PerWL (y = −3.07x + 123.31). In other words, high PerAL, PerBL, or PerWL indicates low LST.

In order to obtain a complete overview of the relationship between LST and LCT, a multiple regression analysis of the relationship between the area ratios of different LCTs and LSTs was conducted (Table 6). The results indicate the contribution of different LCTs to LST. The prediction model is Equation (2):

$$T = k_0 + k_1 CL + k_2 FL + k_3 AL + k_4 WL + k_5 BL \quad (2)$$

where T stands for LST, k_0 is a constant, and k_1–k_5 represent the coefficients of variables.

Table 6. Multivariate linear regression for land surface temperature and land use type area ratio.

Model	No Standardized Coefficient		Standard Coefficient	t	Sig.	R^2
	B	Std. Error				
k_0	36.578	0.328		111.63	0.000	0.928
k_1	0.031	0.004	0.534	8.69	0.000	
k_2	−0.018	0.011	−0.048	−1.632	0.104	
k_3	−0.019	0.004	−0.282	−4.781	0.000	
k_4	−0.048	0.007	−0.230	−6.864	0.000	
k_5	0.001	0.018	0.001	0.039	0.969	

According to Table 6, the model is significant (R^2 = 92.8%). The model expression is shown in Equation (3):

$$T = 36.578 + 0.031CL - 0.018FL - 0.019AL - 0.048WL + 0.001BL \quad (3)$$

The model can be applied to predict LST or adjust the area of various LCTs accordingly to achieve optimal land use planning.

3.4. Quantitative Study of LST and Landscape Patterns of LCTs

The quantitative relationship between LST and the landscape pattern of each LCT was studied based on data of 3 August 2015.

The proportion of BL is relatively small compared to the other types, so it is not sufficient to analyze the relationship between its landscape pattern index and LST at the type level. Therefore, only the relationships between LST and the landscape pattern indices of WL, GL, CL, and AL were analyzed.

The Pearson correlation analysis between the landscape pattern of each LCT and LST is shown in Table 7. The regressive fitting curve of each LCT landscape pattern is shown in Figures 6–9.

Table 7. Pearson correlation between LST and land use at landscape level.

LST of LCTs	PLAND	NP	LPI	LSI	ENN_MN
T_{GL}	−0.149	0.368 *	−0.034	−0.340 *	0.578 **
T_{CL}	0.904 **	−0.730 **	0.890 **	0.513 **	−0.255 *
T_{AL}	−0.789 **	0.274 *	−0.768 **	−0.450 **	0.409 **
T_{WL}	−0.603 **	0.523 **	−0.317 *	−0.671 **	0.588 **

Note: ** Significant at 0.01 level (bidirectional); * significant at 0.05 level (bidirectional).

According to Figure 6, the curve fitting between ENN_MN, LSI, NP, and LST of GL is significant.

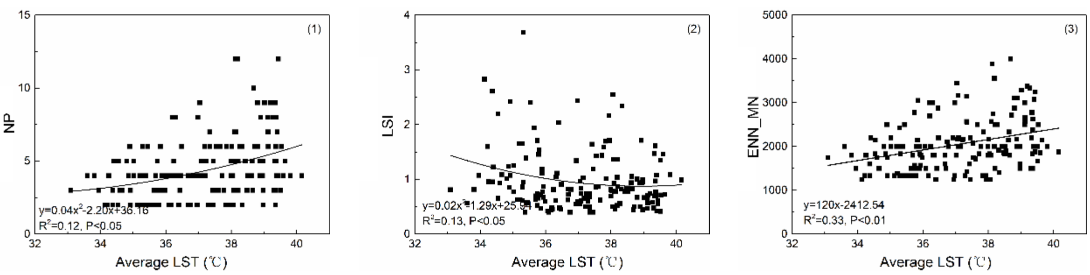

Figure 6. Linear fitting relationship between average land surface temperature and green space (GL) landscape pattern index.

According to Figure 7, PLAND (y = 14.59x − 491.09) and LPI (y = 131x^2 − 79.68x + 1189.93) of CL are well fitted to the LST curve (R^2 > 0.80). NP (y = −2.65x + 104.95) and LSI (y = 0.34x − 8.57) have significant fitting with average LST.

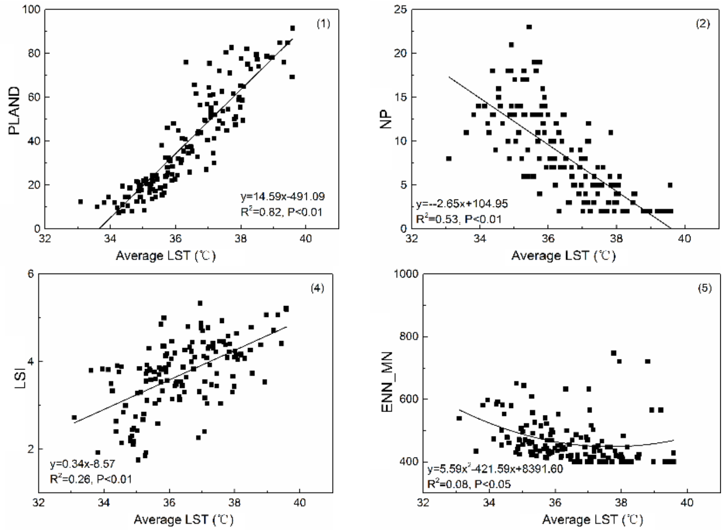

Figure 7. Linear fitting relationship between average land surface temperature and construction land (CL) landscape pattern index.

According to Figure 8, PLAND ($y = -11.34x + 453.85$), LPI ($y = -0.17x^2 + 1.68x + 202.91$), and LSI ($y = -0.13x^2 + 9.29x - 162.12$) of AL have significant fitting with their average LST.

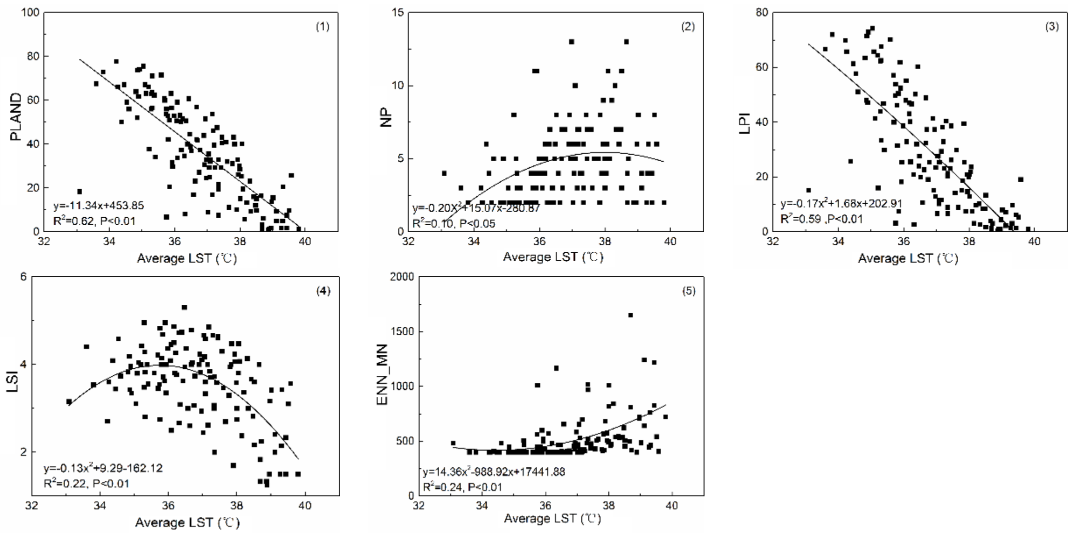

Figure 8. Linear fitting relationship between average land surface temperature and agricultural land (AL) landscape pattern index.

Figure 9 indicates that PLAND ($y = -3.50x + 140.64$), NP ($y = 1.84x - 57.65$), LSI ($y = -0.43x + 19.22$), and ENN_MN ($y = 33.25x^2 - 2331.89x + 41363.84$) of WL have significant fitting with their average LST.

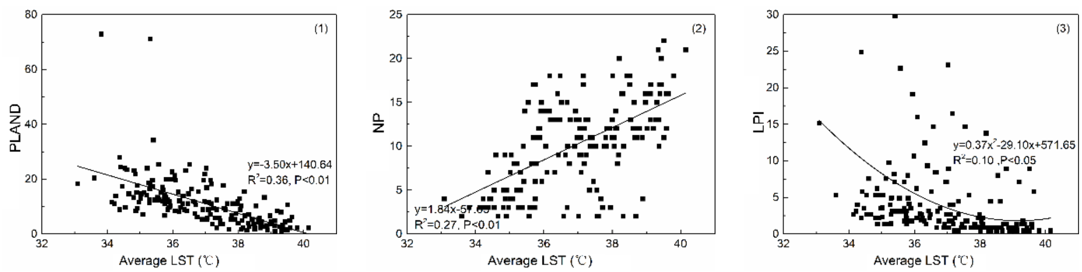

Figure 9. *Cont.*

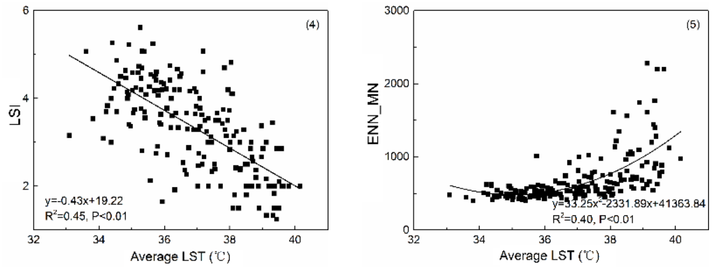

Figure 9. Linear fitting relationship between average land surface temperature and water (WL) landscape pattern index.

4. Discussion

4.1. Thermal Environment of Shanghai

Figure 4 indicates that the UHI effects in Shanghai have become stronger over the years. In 2000, the UHI was only concentrated in the central districts. In 2004, the cool area was further broken down, the UHI extended outside the central district, and UHIs of suburban areas started to form. In 2007, the UHI continued expanding, and most major towns in the western and eastern suburban areas showed significant UHI effects. The cool area was further fragmented. In 2015, the entire main district and suburban area showed strong UHI effects, and the thermal environment became serious.

4.2. LST Differences with LCT

Different LCTs have different absorption and reflection of solar radiation, so their contribution to the LST is significantly different [29]. The surface material of CL is mainly made of asphalt and bricks, which have the lowest thermal capacity and the highest LST [30]. The surface material of BL is mainly natural soil, with strong water permeability. Compared to the artificial impermeable surfaces of CL, BL has a higher thermal inertia and thermal capacity, so its surface temperature is lower than that of CL. GL has a high thermal capacity and strong transpiration and shading effect, so its LST is relatively low [31]. AL is mainly covered by crops and soil. The shading, transpiration, and evaporation effects of moist soil can reduce the LST. However, AL is mainly distributed in the suburbs, where the surrounding LST is already low, so the LST of AL is only slightly lower than that of GL. WL has the strongest evapotranspiration and maximum heat capacity and reflection rate of the above five LCTs. Thus, it has the lowest LST [32].

4.3. Relationship Between LST and Underlying Landscape Pattern

High fragmentation means dispersed GL distribution and long distances between patches. These will result in a high LST [9]. The complex shape of the GL landscape brings a low LST. Centralized distribution of GL patches is more effective at UHI mitigation than scattered patches [33,34]. The more complex the GL patch shape, the lower the LST. The reason for this is that complex GL has more surfaces to exchange energy with the outside, which reduces the temperature of the external environment [31].

According to Table 7, the LST of CL is significantly correlated with the five selected landscape pattern indices ($p < 0.05$). CL is positively correlated with PLAND and LPI and negatively correlated with NP, LSI, and ENN_MN. The reason is that large PLAND and LPI means a large proportion of CL in the area and concentrated distribution, thus the average LST is high. Large NP and ENN_MN means fragment distribution and dispersed distribution of CL, thus the average LST is low. Large LSI means a complex shape of CL, which leads to massive surface contact with the surroundings. Then the thermal energy can be well exchanged, thus increasing the average LST around it.

The average temperature of AL is significantly lower than that of the whole city, so AL has the function of reducing the LST and alleviating UHI effects. Large PLAND and LPI values indicate a high proportion and concentrated distribution of AL in the selected area, so the average LST is low. Large NP and ENN_MN lead to a serious degree of fragmentation and dispersed distribution of AL, so the average LST is high. A large LSI indicates a complex shape of AL, which brings more contact with the outside, thus more effective average LST reduction can be achieved. To sum up, large patch area, concentrated distribution, and complex shape of AL result in low average LST and significant relief from UHI effects.

The average temperature of WL is significantly lower than that of the whole surface, so WL can reduce the LST and alleviate UHI effects [35]. Large PLAND and LPI values indicate a high area ratio and concentrated distribution of WL in the area, which results in a low average LST. High NP and ENN_MN mean serious fragmentation and dispersed distribution of WL. This leads to a high average LST. A large LSI indicates a complex shape of WL and more external surface contact with the surroundings. This results in an effective reduction of average LST. In other words, large patch area, concentrated distribution, and complex shape of WL result in a low average LST and significant relief from UHI effects.

5. Conclusions

In this paper, multidisciplinary theories and methods were applied to study the impact of LCTs and their configurations on the LST of the megacity of Shanghai. The results show that the thermal environment of Shanghai has become worse over the years. The LSTs of different LCTs are significantly different. The average LST ranking of LCTs is CL > BL > GL > AL > WL. CL contributes the most to the UHI effect and forms heat island centers easily, while WL and GL have significant effects on relieving UHI effects and form cold island centers easily. For GL, WL, and AL, a large area, a small degree of fragmentation, concentrated distribution, and complex shape lead to low average LST rankings and strong mitigation of the UHI. For CL, the effect is the opposite, which means that a large area, a small degree of fragmentation, concentrated distribution, and a complex shape lead to a high average LST and obvious UHI effect. Therefore, to carry out effective landscape planning in order to mitigate UHI effects as much as possible, CL should be distributed in as many discrete pieces as possible, and large areas of CL should be broken up by GL or WL, which can effectively alleviate UHI effects. The study helps with the understanding of the UHI in Shanghai and provides a reference basis for authorities to formulate targeted strategies to alleviate UHI effects.

In further study, the following points still need to be addressed:

(1) The correlation analysis between LST and LCT landscape patterns can be improved by introducing multivariate analysis. Principal component analysis can also be introduced to avoid correlation of the variants.

(2) The most frequently applied landscape indices for LCT are used in this study without justification. More indices may influence the LST of the LCT and should be evaluated.

Author Contributions: Conceptualization, H.D. and Y.C.; methodology, P.L.; RS figure processing, H.D. and J.A; validation H.J.; writing—original draft preparation, H.D.; writing—review and editing, H.D.; project administration, H.D.; funding acquisition, H.D.

Funding: The research was supported by the Shanghai Social Science Planning Youth Project (2018ECK003) and National Natural Science Foundation of China (grant no. 31670474).

Acknowledgments: The authors would like to express their sincere thanks to research assistants, who provided assistance with the field measurements.

Conflicts of Interest: The authors declare no conflict of interest.

References

1. Oke, T.R. City size and the urban heat island. *Atmos. Environ.* **1973**, *7*, 769–779. [CrossRef]
2. Lo, C.P.; Quattrochi, D.A.; Luvall, J.C. Application of high-resolution thermal infrared remote sensing and GIS to assess the urban heat island effect. *Int. J. Remote Sens.* **1997**, *18*, 287–304. [CrossRef]

3. Coseo, P.; Larsen, L. How factors of land use/land cover, building configuration, and adjacent heat sources and sinks explain urban heat islands in Chicago. *Landsc. Urban Plan.* **2014**, *125*, 117–129. [CrossRef]
4. Debbage, N.; Shepherd, J.M. The urban heat island effect and city contiguity. *Comput. Environ. Urban Syst.* **2015**, *54*, 181–194. [CrossRef]
5. Guo, G.; Wu, Z.; Xiao, R.; Chen, Y.; Liu, X.; Zhang, X. Impacts of urban biophysical composition on land surface temperature in urban heat island clusters. *Landsc. Urban Plan.* **2015**, *135*, 1–10. [CrossRef]
6. Deng, Y.; Wang, S.; Bai, X.; Tian, Y.; Wu, L.; Xiao, J.; Chen, F.; Qian, Q. Relationship among land surface temperature and LUCC, NDVI in typical karst area. *Sci. Rep.* **2018**, *8*, 641. [CrossRef] [PubMed]
7. Guha, S.; Govil, H.; Dey, A.; Gill, N. Analytical study of land surface temperature with NDVI and NDBI using Landsat 8 OLI and TIRS data in Florence and Naples city, Italy. *Eur. J. Remote Sens.* **2018**, *51*, 667–678. [CrossRef]
8. Pal, S.; Ziaul, S. Detection of land use and land cover change and land surface temperature in English Bazar urban center. *Egypt. J. Remote Sens. Space Sci.* **2017**, *20*, 125–145.
9. Li, X.; Zhou, W.; Ouyang, Z.; Xu, W.; Zheng, H. Spatial pattern of greenspace affects land surface temperature: Evidence from the heavily urbanized Beijing metropolitan area, China. *Landsc. Ecol.* **2012**, *27*, 887–898. [CrossRef]
10. Peng, J.; Xie, P.; Liu, Y.; Ma, J. Urban thermal environment dynamics and associated landscape pattern factors: A case study in the Beijing metropolitan region. *Remote Sens. Environ.* **2016**, *173*, 145–155. [CrossRef]
11. Maimaitiyiming, M.; Ghulam, A.; Tiyip, T.; Pla, F.; Latorre-Carmona, P.; Halik, Ü.; Sawut, M.; Caetano, M. Effects of green space spatial pattern on land surface temperature: Implications for sustainable urban planning and climate change adaptation. *ISPRS J. Photogramm. Remote Sens.* **2014**, *89*, 59–66. [CrossRef]
12. Asgarian, A.; Amiri, B.J.; Sakieh, Y. Assessing the effect of green cover spatial patterns on urban land surface temperature using landscape metrics approach. *Urban Ecosyst.* **2015**, *18*, 209–222. [CrossRef]
13. Sun, R.; Chen, L. Effects of green space dynamics on urban heat islands: Mitigation and diversification. *Ecosyst. Serv.* **2017**, *23*, 38–46. [CrossRef]
14. Chapman, L.; Bell, C.; Bell, S. Can the crowdsourcing data paradigm take atmospheric science to a new level? A case study of the urban heat island of London quantified using Netatmo weather stations. *Int. J. Climatol.* **2017**, *37*, 3597–3605. [CrossRef]
15. Rizwan, A.M.; Dennis, L.Y.; Chunho, L.I.U. A review on the generation, determination and mitigation of Urban Heat Island. *J. Environ. Sci.* **2008**, *20*, 120–128. [CrossRef]
16. Giannaros, C.; Nenes, A.; Giannaros, T.M.; Kourtidis, K.; Melas, D. A comprehensive approach for the simulation of the Urban Heat Island effect with the WRF/SLUCM modeling system: The case of Athens (Greece). *Atmos. Res.* **2018**, *201*, 86–101. [CrossRef]
17. Bonafoni, S.; Baldinelli, G.; Verducci, P. Sustainable strategies for smart cities: Analysis of the town development effect on surface urban heat island through remote sensing methodologies. *Sustain. Cities Soc.* **2017**, *29*, 211–218. [CrossRef]
18. Bai, Y.; Wang, X.Y.; Jiang, H.M.; Liu, S.D. Progress of urban heat island effect. *J. Meteorol. Environ.* **2013**, *2*, 101–106.
19. Murphy, D.J.; Hall, M.H.; Hall, C.A.; Heisler, G.M.; Stehman, S.V.; Anselmi-Molina, C. The relationship between land cover and the urban heat island in northeastern Puerto Rico. *Int. J. Climatol.* **2011**, *31*, 1222–1239. [CrossRef]
20. Rao, P.K. Remote sensing of urban "heat islands" from an environmental satellite. *Bull. Am. Meteorol. Soc.* **1972**, *53*, 647–648.
21. Zhang, K.; Wang, R.; Shen, C.; Da, L. Temporal and spatial characteristics of the urban heat island during rapid urbanization in Shanghai, China. *Environ. Monit. Assess.* **2010**, *169*, 101–112. [CrossRef]
22. Wang, H.; Zhang, Y.; Tsou, J.Y.; Li, Y. Surface urban heat island analysis of Shanghai (China) based on the change of land use and land cover. *Sustainability* **2017**, *9*, 1538. [CrossRef]
23. Huang, W.; Li, J.; Guo, Q.; Mansaray, L.R.; Li, X.; Huang, J. A Satellite-derived climatological analysis of urban heat island over Shanghai during 2000–2013. *Remote Sens.* **2017**, *9*, 641. [CrossRef]
24. Zhou, H.M.; Gao, Y.; Ge, W.Q.; Li, T.T. The research on the relationship between the urban expansion and the change of the urban heat island distribution in Shanghai area. *Ecol. Environ.* **2008**, *17*, 163–168.
25. Qi, L. Trend Analysis of Midsummer High Temperature and Urban Heat Island Effect in Shanghai over Past 10 Years. *Meteorol. Sci. Technol.* **2004**, *32*, 433–437. (In Chinese)

26. Tan, J.; Zheng, Y.; Tang, X.; Guo, C.; Li, L.; Song, G.; Zhen, X.; Yuan, D.; Kalkstein, A.J.; Li, F. The urban heat island and its impact on heat waves and human health in Shanghai. *Int. J. Biometeorol.* **2010**, *54*, 75–84. [CrossRef]
27. Du, H.; Wang, D.; Wang, Y.; Zhao, X.; Qin, F.; Jiang, H.; Cai, Y. Influences of land cover types, meteorological conditions, anthropogenic heat and urban area on surface urban heat island in the Yangtze River Delta Urban Agglomeration. *Sci. Total Environ.* **2016**, *571*, 461–470. [CrossRef]
28. Tuia, D.; Volpi, M.; Copa, L.; Kanevski, M.; Munoz-Mari, J. A survey of active learning algorithms for supervised remote sensing image classification. *IEEE J. Sel. Top. Signal Process.* **2011**, *5*, 606–617. [CrossRef]
29. Zhou, S.Z.; Shu, J. *Urban Climatology*; China Meteorological Press: Beijing, China, 1994. (In Chinese)
30. Jin, M.S.; Kessomkiat, W.; Pereira, G. Satellite-observed urbanization characters in Shanghai, China: Aerosols, urban heat island effect, and land–atmosphere interactions. *Remote Sens.* **2011**, *3*, 83–99. [CrossRef]
31. Cao, X.; Onishi, A.; Chen, J.; Imura, H. Quantifying the cool island intensity of urban parks using ASTER and IKONOS data. *Landsc. Urban Plan.* **2010**, *96*, 224–231. [CrossRef]
32. Imhoff, M.L.; Zhang, P.; Wolfe, R.E.; Bounoua, L. Remote sensing of the urban heat island effect across biomes in the continental USA. *Remote Sens. Environ.* **2010**, *114*, 504–513. [CrossRef]
33. Wong, N.H.; Yu, C. Study of green areas and urban heat island in a tropical city. *Habitat Int.* **2005**, *29*, 547–558. [CrossRef]
34. Oliveira, S.; Andrade, H.; Vaz, T. The cooling effect of green spaces as a contribution to the mitigation of urban heat: A case study in Lisbon. *Build. Environ.* **2011**, *46*, 2186–2194. [CrossRef]
35. Sun, R.; Chen, A.; Chen, L.; Lü, Y. Cooling effects of wetlands in an urban region: The case of Beijing. *Ecol. Indic.* **2012**, *20*, 57–64. [CrossRef]